Charge separation in Coulomb liquids: mean-spherical approximation and Monte Carlo simulation

1999 J. Phys.: Condens. Matter 11 3019

(http://iopscience.iop.org/0953-8984/11/15/008)

J. Phys.: Condens. Matter **11** (1999) 3019–3028. Printed in the UK PII: S0953-8984(99)97677-4

Charge separation in Coulomb liquids: mean-spherical approximation and Monte Carlo simulation

Thorsten Koslowski and Uta Beck

Institut für Physikalische Chemie I, Universität Karlsruhe, Kaiserstraße 12, D-76128 Karlsruhe, Germany

Received 18 September 1998, in final form 27 January 1999

Abstract. With reference to dense ionic liquids like the alkali metal–alkali halide melts, $M_x[MX]_{1-x}$, we present a study of the distribution of the excess electronic charge x in Coulomb systems with electronic degrees of freedom. Within the mean-spherical approximation to the restricted primitive model of ionic liquids, we demonstrate the stability of systems that exhibit a maximum separation of cationic charges, $z_M \in \{0, 1\}$. The results are verified and illustrated by Monte Carlo simulations. We discuss the implications of the principle of maximum charge separation for the electronic structure and the thermodynamics of dense ionic liquids, possible additional applications and its limitations due to the neglect of quantum effects.

1. Introduction

Alkali metal–alkali halide melts $M_x[MX]_{1-x}$ (M = Li, Na, K, Rb, Cs; X = F, Cl, Br, I) are a subject of current interest in physics and physical chemistry, in particular as regards their microscopic and electronic structure [1]. For the prototypical K–KCl system, experimental work covers neutron scattering [2], NMR studies on the related Cs halides [3], conductivity measurements [4], ESR spectroscopy [5], the determination of optical absorption properties [6], ellipsometric studies [7], small-angle x-ray scattering [8] and the measurement of thermodynamic data [9].

For K–KCl, the following picture emerges with increasing excess metal concentration x. For small values of x, excess electrons populate defect states like F centres or spin-paired bipolarons. They can be characterized by an optical absorption process from a localized ground state of s symmetry to a localized excited p state, giving rise to an absorption band that can be described by a Gaussian line shape [6]. Even for the smallest excess metal concentrations, a second, Drude-like component can be observed in the frequency-dependent complex dielectric response [7]. It is usually attributed to weakly localized electrons, which should make a considerable contribution to the electronic conductivity. The schematic theoretical density of states originating from this picture is presented in figure 1 [10]. With x increasing further, the alkali metal conduction band is populated. The system undergoes a continuous non-metal–metal transition at $x \simeq 0.2$–0.3 [1] and thus changes the character of the chemical bond from ionic to metallic. In addition to a large amount of experimental evidence, quantum path integral simulations [11] and *ab initio* molecular dynamics studies of the Car–Parrinello type [12] support this interpretation.

An important problem is posed by the electronic degree of freedom inherent to the system even in the absence of F centres. The excess electronic charge can either be completely

0953-8984/99/153019+10$19.50

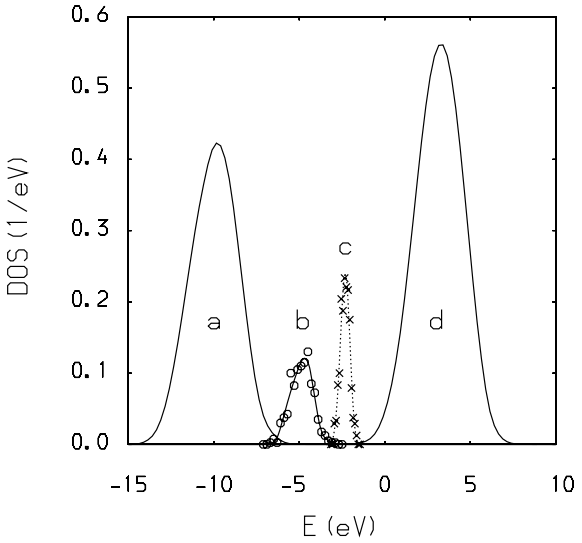

Figure 1. A schematic density of states including defect levels in the regime of a small excess metal concentration. The chlorine valence band (a), F-centre ground state (b), F-centre excited state (c) and potassium conduction band (d). The energy is in electron volts, and the density of states is per electron volt and atom. After [10].

delocalized over all metal cations—a picture appropriate in the metallic regime—or may be localized on individual metal atoms, a behaviour that is usually attributed to the low-x regime. Disorder-induced Anderson localization of eigenstates [13] in ionic liquids is favoured by the presence of spatial fluctuations in the Coulombic energy [14]:

$$V_{\mathrm{M};i} = \frac{e^2}{4\pi\epsilon_0} \sum_{j \neq i} \frac{z_i z_j}{r_{ij}}. \tag{1.1}$$

As argued by Logan and Siringo [14], the spatially disordered distribution of ions in a liquid with charge transfer leads to strong local fluctuations in the local Madelung fields ($\sim$1 eV) potentially experienced by an electron as it hops between the cations.

In the article of Logan and Siringo and in subsequent numerical work [10,16], the so-called restricted primitive model (RPM) of ionic liquids, comprising hard-sphere ions that interact via point charges, has been applied:

$$V(r) = \begin{cases} \infty & \text{for } r < \sigma \\ \dfrac{e^2 z_i z_j}{4\pi\epsilon_0 r} & \text{for } r \geqslant \sigma. \end{cases} \tag{1.2}$$

For convenience, the calculation of the Coulombic site energies—entering the diagonal energies of a tight-binding Hamiltonian—has been based upon a homogeneously distributed cationic charge, $z_{\mathrm{M}} = 1 - x$, both in analytical and numerical computations of the electronic structure of ionic liquids and charge-transfer alloys. In the low-x regime, however, electronic eigenstates are localized in the conduction band tail down to the regime of so-called quasiatomic states [15], leading to an obvious inconsistency. We will refer to this inconsistency as the *localization dilemma*.

From a theoretical perspective, the thermodynamic properties of alkali–alkali halide melts have been addressed by Dijkstra *et al* [17] and by Holzhey and Schirmacher [18]. Recently, Freyland and the present authors [19] have utilized Ginoza's screened mean-spherical approximation [20]—as suggested by Yurdabak *et al* [21]—to describe the non-metal $\rightarrow$ metal crossover in the K–KCl system in terms of a balance between strongly localized electrons populating F centres and nearly free electrons.

In this article, we address the question of the homogeneous or heterogeneous nature of the distribution of the excess electronic charge from an analytical and a numerical point of view. We are thus restricted to the RPM as one of the few models relevant to ionic liquids that is analytically tractable within the MSA. It is essential to note that we work within a purely classical model and completely neglect quantum mechanical degrees of freedom.

The remainder of the article is organized as follows. In the next section, we demonstrate that within the mean-spherical approximation (MSA), the RPM exhibits a heterogeneous charge distribution. In the third section, the Monte Carlo algorithm underlying the computer simulations is presented. Numerical and simulation results relevant to the parameter range of dense ionic liquids are presented and discussed in the fourth section, and conclusions are derived in the final section.

2. Mean-spherical approximation

The Ornstein–Zernike (OZ) equation

$$h_{ij}(r) \equiv g_{ij}(r) - 1 = c_{ij}(r) + \rho \sum_k x_k \int c_{ik}(|\boldsymbol{r} - \boldsymbol{r}'|) h_{kj}(r')\, \mathrm{d}\boldsymbol{r}' \tag{2.1}$$

forms the basis of the theoretical treatment of multicomponent liquids [22]. The radial pair distribution functions, $g_{ij}(r)$, are expressed in terms of the direct correlation functions, $c_{ij}(r)$. For the restricted primitive model, all ionic hard-sphere diameters are identical, and $h_{ij}(r) = -1$ for $r < \sigma$ holds. Within the MSA, a closure relation for the OZ integral equation is introduced by approximating the direct correlation function by

$$c_{ij}(r) = -\frac{\beta e^2 z_i z_j}{4\pi\epsilon_0 r}. \tag{2.2}$$

The details of the computation have been presented by Blum and Høye [23]. The results can be expressed in terms of the MSA screening constant

$$\Gamma = \frac{-1 + \sqrt{1 + 2\sigma\kappa}}{2\sigma} \tag{2.3}$$

which only depends on the hard-sphere diameter σ and on the Debye screening constant,

$$\kappa = \sqrt{\frac{\beta e^2}{\epsilon_0} \sum_i \rho_i z_i^2}. \tag{2.4}$$

The MSA internal energy equals

$$\Delta U = -\frac{e^2\rho}{4\pi\epsilon_0} \underbrace{\frac{\Gamma}{1 + \Gamma\sigma}}_{A} \underbrace{\sum_i \frac{\rho_i z_i^2}{\rho}}_{B}. \tag{2.5}$$

$2A$ can be interpreted as the equivalent of a Madelung constant for the liquid state; B is introduced here as a convenient abbreviation.

For a homogeneous charge distribution, global charge neutrality and stoichiometry constraints lead for the $M_x[MX]_{1-x}$ system to the following ionic charges and partial densities: $z_X = -1$, $\rho_X/\rho = (1-x)/(2-x)$, $z_M = (1-x)$ and $\rho_M/\rho = 1/(2-x)$. Inserting these quantities into the definitions of the Debye screening constant, equation (2.4), and computing Γ using equation (2.3), we arrive at

$$\Gamma_H = \left[-1 + \sqrt{1 + 2\sigma\sqrt{D(1-x)}} \right] \Big/ 2\sigma \tag{2.6}$$

with $D = \beta e^2 \rho/\epsilon_0$ and $\sqrt{[D(1-x)]} = \kappa_{\mathrm{H}}$. The subscript distinguishes the case of a homogeneous (H) from that of an inhomogeneous (I) charge distribution. For B, as defined in equation (2.5), we arrive at

$$B_{\mathrm{H}} = B_{\mathrm{H}}^{-} + B_{\mathrm{H}}^{+} = \frac{1-x}{2-x}(-1)^2 + \frac{1}{2-x}(1-x)^2 = \frac{2-3x+x^2}{2-x}. \tag{2.7}$$

The case of the inhomogeneous charge distribution can be characterized by $z_{\mathrm{X}} = -1$, $\rho_{\mathrm{X}}/\rho = (1-x)/(2-x)$, $z_{\mathrm{M}^+} = +1$, $\rho_{\mathrm{M}^+}/\rho = (1-x)/(2-x)$, $z_{\mathrm{M}^0} = 0$, $\rho_{\mathrm{M}^0}/\rho = x/(2-x)$. With

$$\kappa_{\mathrm{I}} = \sqrt{2D(1-x)/(2-x)}$$

we arrive at a MSA screening constant

$$\Gamma_{\mathrm{I}} = \left[-1 + \sqrt{1 + 2\sigma\sqrt{2D(1-x)/(2-x)}} \right] \Big/ 2\sigma. \tag{2.8}$$

We note that

$$B_{\mathrm{I}} = B_{\mathrm{I}}^{-} + B_{\mathrm{I}}^{+} + B_{\mathrm{I}}^{0} = \frac{1-x}{2-x}(-1)^2 + \frac{1-x}{2-x}(+1)^2 + \frac{x}{2-x}0^2 = \frac{2(1-x)}{2-x}. \tag{2.9}$$

It immediately follows that

$$\frac{B_{\mathrm{H}}}{B_{\mathrm{I}}} = \frac{2-3x+x^2}{2(1-x)} = 1 - \frac{x}{2} \leqslant 1. \tag{2.10}$$

Γ_{I} and Γ_{H} only differ in their Debye screening constants, κ. As $\kappa_{\mathrm{H}} = 2\kappa_{\mathrm{I}}/(2-x)$ and as it appears as a positive quantity in the numerator of the Γ formula (equations (2.3), (2.6), (2.8), we note that $\Gamma_{\mathrm{I}} \geqslant \Gamma_{\mathrm{H}}$. Consequently, the following inequality holds:

$$\frac{A_{\mathrm{H}}}{A_{\mathrm{I}}} = \frac{\Gamma_{\mathrm{H}}}{\Gamma_{\mathrm{I}}}\frac{1+\Gamma_{\mathrm{I}}\sigma}{1+\Gamma_{\mathrm{H}}\sigma} = \frac{\Gamma_{\mathrm{H}} + \Gamma_{\mathrm{H}}\Gamma_{\mathrm{I}}\sigma}{\Gamma_{\mathrm{I}} + \Gamma_{\mathrm{H}}\Gamma_{\mathrm{I}}\sigma} \leqslant 1. \tag{2.11}$$

As both $A_{\mathrm{H}}/A_{\mathrm{I}}$ and $B_{\mathrm{H}}/B_{\mathrm{I}}$ are smaller than or equal to unity, the same statement holds for the corresponding ratio of the internal energies, $U_{\mathrm{H}}/U_{\mathrm{I}} \propto (A_{\mathrm{H}}B_{\mathrm{H}})/(A_{\mathrm{I}}B_{\mathrm{I}})$ (cf. equation (2.5)).

Within the MSA, the free energy of the model system at constant volume, temperature and particle number (NVT) is given by

$$\Delta F = \Delta U + \frac{k_{\mathrm{B}}T}{3\pi\rho}\Gamma^3 + k_{\mathrm{B}}T\sum_i x_i \ln x_i. \tag{2.12}$$

In the dilute regime ($\Gamma\sigma = 0$), the first two terms on the right-hand side of equation (2.12) can be reduced to

$$\Delta F = -\frac{1}{3}\left(\frac{e^2 B}{4\pi\epsilon_0}\right)^{3/2}\left(\frac{\rho}{k_{\mathrm{B}}T}\right)^{1/2} \tag{2.13}$$

As shown above (equation (2.10)), B_{H} is smaller than B_{I} and, consequently, the system characterized by an inhomogeneous charge distribution is stabilized with respect to its homogeneous counterpart. The assumption that ΔS is given by the ideal entropy of mixing—as expressed in equation (2.12)—leads to an additional stabilization. Considering the numerical results for ΔF in the high-density regime described below and the conclusions derived from the dilute regime, it is not completely unlikely that an inhomogeneous charge distribution is also stabilized in the intermediate regime. It goes without saying that this assumption—even if substantiated by numerical evaluations of the MSA scheme—cannot replace a rigorous proof.

Regardless of the density, the free energy can be expanded as a Taylor series around $x = 0$. We introduce the constants $C = e^2/4\pi\epsilon_0$, $E = k_{\mathrm{B}}T/3\pi\rho$ and the expression

$$Q = \sqrt{1 + 2\sigma\sqrt{D}} \tag{2.14}$$

which is larger than unity for any non-trivial ionic density, $\rho > 0$. Considering that $\Gamma = f(x)$, we arrive at

$$\Delta F_{\mathrm{I}} = \Delta F\big|_{x=0} + \frac{\sqrt{D}}{8}\frac{4C + 8CQ - 3ED}{1+Q^3}x + \mathrm{O}(x^2) \tag{2.15}$$

and

$$\Delta F_{\mathrm{H}} = \Delta F\big|_{x=0} + \frac{\sqrt{D}}{8}\frac{8C + 4CQ - 6ED}{1+Q^3}x + \mathrm{O}(x^2) \tag{2.16}$$

for the first two terms on the right-hand side of equation (2.12). With $Q > 1$, $C > 0$ and $E \geqslant 0$, it is straightforward to demonstrate that the initial slope of $\Delta F_{\mathrm{H}}(x)$ is larger than that of $\Delta F_{\mathrm{I}}(x)$. This behaviour again indicates the relative stabilization induced by an inhomogeneous charge distribution.

Within the mean-spherical approximation, we have thus demonstrated that the internal energy ΔU of the restricted primitive model of ionic fluids of the type $\mathrm{M}_x[\mathrm{MX}]_{1-x}$ is lowered by replacing the homogeneous cationic charge distribution $z_{\mathrm{M}} = 1 - x$ by charges of unity and zero. Both energies are trivially equal only in the limits of the pure metallic ($x = 1$) and the pure ionic ($x = 0$) regimes. The free energy exhibits the same features in the low-density regime and—independent of the density—for small excess metal concentrations x.

3. Monte Carlo simulations

To model the microscopic structure of the primitive model of ionic fluids, we have applied the standard Metropolis Monte Carlo (MC) algorithm [24]. The systems are simulated at constant particle number, volume and temperature (NVT). For each excess metal concentration x, we have performed 5000 MC steps to equilibrate the system, and a further 5000 steps to compute averages. A Monte Carlo step is the attempt to move each ion once on average. The Adams cut-off strategy is used to enforce local charge neutrality [25]. The experimental densities as extrapolated to $p = 1$ bar [26] have been used. Details of the systems simulated are listed in table 1.

Table 1. Simulated systems (432 atoms), Madelung potentials V_{M} and their RMS fluctuations, ΔV_{M}, for electronic test charges.

x	Number of anions	V_{mol} (cm^3)	$V_{\mathrm{M}^+} \pm \Delta V_{\mathrm{M}^+}$	$V_{\mathrm{M}^-} \pm \Delta V_{\mathrm{M}^-}$	ΔV_{M^0}
0.000	216	51.36	8.23 ± 0.84	-8.22 ± 0.84	—
0.094	205	51.97	8.28 ± 0.87	-8.25 ± 0.84	0.86
0.145	199	53.03	8.22 ± 0.86	-8.28 ± 0.87	0.81
0.226	188	54.16	8.26 ± 0.85	-8.25 ± 0.82	0.82
0.335	173	56.09	8.23 ± 0.86	-8.26 ± 0.87	0.80
0.444	154	57.38	8.28 ± 0.89	-8.26 ± 0.86	0.79
0.631	116	58.49	8.29 ± 0.90	-8.19 ± 0.87	0.79
0.827	64	60.35	7.94 ± 0.99	-8.03 ± 1.03	0.79

The cationic charges z_{M} are allowed to vary continuously between zero and unity, with the constraint of global charge neutrality. Starting from a uniform cationic charge distribution $z_{\mathrm{M}} = 1-x$, small packets of charges δz_{M} are allowed to hop between the cations. The quantity δz_{M} is drawn from a box distribution in the interval [0, 0.1], and charge transfer between cations is accepted or rejected according to the Metropolis MC rules. In addition, a charge-transfer step is rejected if it leads to a cationic charge smaller than zero or larger than unity. As is common

for systems that exhibit electronic degrees of freedom, we use a two-thermostat strategy [27]: the ionic degrees of freedom are simulated at the actual temperature (here: $k_{\mathrm{B}}T = 0.101$ eV), whereas the electronic degrees of freedom are coupled to a low-temperature heat bath at 5 K. For each particle trial move, ten attempts to transfer cationic charges have been performed.

4. Numerical results and discussion

In figure 2, we present numerical results for the internal energy per ion, ΔU, and the free energy per ion, ΔF, as functions of the excess metal concentration x [30]. The free energy has been evaluated at constant temperature, volume and particle number. Energy values have been obtained within the MSA for a homogeneous charge distribution, $z_{\mathrm{M}} = 1 - x$, and a binodal charge distribution, $z_{\mathrm{M}} \in \{0, 1\}$. The Monte Carlo simulations described in the last section rapidly converge to the binodal charge distribution used for the inhomogeneous MSA computations. For all systems studied, the maximum accepted charge transfer after equilibration amounts to $\delta z_{\mathrm{M}} = 1 \times 10^{-3}$. The two peaks of the charge distribution show a maximum RMS fluctuation of $\Delta z_{\mathrm{M}} = 2.5 \times 10^{-3}$. In addition, we have performed Monte Carlo simulations with fixed homogeneous cationic charges. For both types of MC simulation, the internal energy as a function of x is shown in figure 2. As is evident from this figure, the energetics of the MSA is in good agreement with the corresponding MC results. Both the MSA results and the computer simulations clearly indicate the strong stabilization of the model characterized by a binodal charge distribution with reference to a homogeneous charge distribution. At $x = 1/2$, the MSA stabilization energy amounts to slightly more than half an electron volt. The free energy as a function of excess metal concentration exhibits the same tendency as the internal energy: ΔF_{I} and ΔF_{H} are well separated for all but the largest values of x, and $\Delta F_{\mathrm{H}} \geqslant \Delta F_{\mathrm{I}}$.

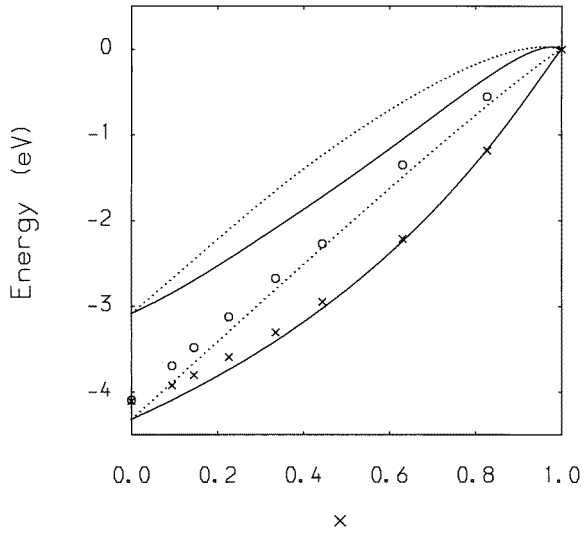

Figure 2. Energy as a function of excess metal concentration. From top to bottom: (a) ΔF, homogeneous charge distribution, MSA (dotted curve); (b) ΔF, binodal charge distribution, MSA (solid curve); (c) ΔU, homogeneous charge distribution, MSA (dotted curve); (d) ΔU, homogeneous charge distribution, MC simulation ($\circ$ symbols); (e) ΔU, binodal charge distribution, MSA (solid curve); (f) ΔU, binodal charge distribution, MC simulation ($\times$ symbols). The energy is in electron volts per ion.

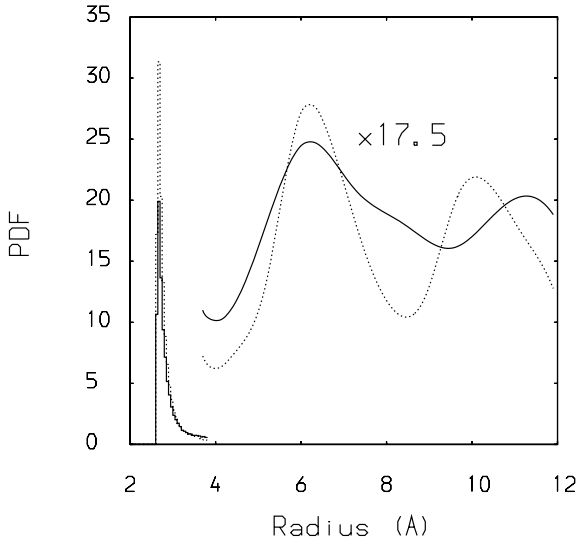

Figure 3. The anion–cation radial pair distribution function at stoichiometry ($x = 0$, solid curve) and for an excess metal concentration of $x = 0.631$ (dotted curve). In the interval from 3.8 to 12 Å, the PDF has been enlarged by a factor of 17.5. The radius is in ångströms.

In figure 3, the cation–anion partial pair distribution function, $g_{+-}(r)$, is presented at stoichiometry and at $x = 0.631$. Both curves exhibit oscillations characteristic of ionic fluids. It is interesting to note that these oscillations are more pronounced in the dilute system. The number of ionic neighbours next to a given ion (defined via a cut-off radius of $r_c = 3.8$ Å) increases from 4.5 at stoichiometry to 6.1 at $x = 0.631$.

In the range of excess metal concentrations $0 \leqslant x \leqslant 0.827$, the Coulombic site energies, V_M, of anions and cations in the binodal charge distribution model vary between 7.94 and 8.29 electron volts. As the total energy of a system comprising equi-sized ions of opposite charge should remain constant upon reversing the sign of all charges, and as neutral particles should on average experience a neutral neighbourhood on all length scales, the average Madelung potential probed by an electronic test charge located on a neutral metal atom equals zero. Like its ionic counterpart it does, however, experience variations in its local environment that lead to Madelung potential fluctuations on the same energy scale as those characteristic of ions, namely. 0.8–0.9 electron volts (see table 1).

For $x = 0.094$, we have computed the electronic structure of the model system using the tight-binding Hamiltonian given by one of the present authors [10, 28, 29]. The model Hamiltonian is characterized by nearest- and next-nearest-neighbour short-range hopping between atomic s and p orbitals. The diagonal elements are the sum of the valence orbital ionization potentials (K) or the electron affinities (Cl), the Madelung potential experienced by an electronic test charge and a polarization contribution [31]. For the three different types of particle present in the model liquid, we arrive at average values of $\epsilon_{s,Cl^-} = -22.21$ eV, $\epsilon_{p,Cl^-} = -10.11$ eV, $\epsilon_{s,K^+} = +1.16$ eV, $\epsilon_{p,K^+} = +2.77$ eV, $\epsilon_{s,K^0} = -4.34$ eV and $\epsilon_{p,K^0} = -2.73$ eV. The resulting density of states—as presented in figure 4—is based upon 50 realizations, each providing 1728 eigenvalues of the Hamiltonian matrix. Similarly to the case for figure 1, the anionic valence band (centred at ~ -10.5 eV) and the cationic conduction band (centred at $\sim +3$ eV) are broadened by electron hopping and Madelung potential disorder [15, 16, 28]. The small band located in the band gap of the stoichiometric compound (at ~ -3 eV) can be unambiguously attributed to neutral potassium (K^0) states. The Fermi level—indicated by a vertical dotted line—lies at $E = -4.68$ eV within the K^0 band, almost coinciding with the centre of the F-centre band ($E = -4.87$ eV [10]), as represented by

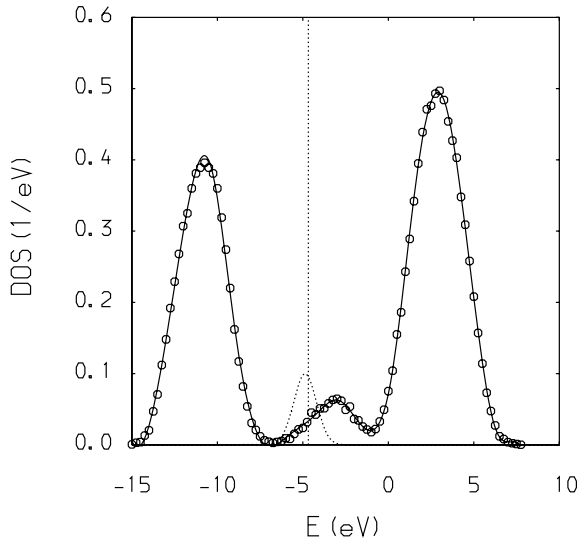

Figure 4. The computed density of states for an excess metal concentration of $x = 0.094$. From left to right: chlorine valence, neutral metal atom and cationic conduction band. The solid curve is a guide to the eye. The Fermi level is indicated by a dotted vertical line. The F-centre ground-state band—as shown in figure 1—is indicated by a dotted curve. The energy is in electron volts, and the density of states is per electron volt and atom.

the dotted curve. This picture is in accord with the experimental observation of the coexistence of eigenstates giving rise to an optical absorption characteristic of F centres and eigenstates that show a Drude-like frequency-dependent dielectric response [6,7]. In contrast to the model characterized by a homogeneous charge distribution, M^0 and F-centre eigenstates coexist at the Fermi level.

5. Conclusions

In this work, we have studied the distribution of the excess electronic charge of systems exhibiting electronic degrees of freedom with reference to alkali metal–alkali halide melts, $M_x[MX]_{1-x}$, within the mean-spherical approximation and by Monte Carlo simulations. Within the MSA, we have been able to demonstrate for the restricted primitive model of equi-sized ions that charge separation is energetically favoured, regardless of the parameters characterizing the model. This result has been confirmed and illustrated using Monte Carlo simulations. In the small-x regime, we have computed the electronic structure of the model system, leading to the formation of a small M^0 band energetically located between the anionic valence and the cationic conduction band, in which the Fermi level now lies. Around the Fermi level, both F-centre and M^0 states exist, in accord with the experimental observation of simultaneous optical absorption between defect states and a Drude-like behaviour of the conduction electrons.

The principle that charge separation is energetically favoured in Coulomb systems with electronic degrees of freedom solves the 'localization dilemma' expressed in the introduction: in the regime of small excess metal concentrations x, the charge distribution used to generate the microscopic geometry of the system is now consistent with the results of the electronic structure computation that is based upon this geometry.

The range of validity of this principle is obviously limited to the regime where significant broadening of the binodal charge distribution by thermal effects or by electron hopping can be neglected. In the latter case, the kinetic energy of the delocalized electrons leads to the formation of bands and compensates for the energy difference between systems with homogeneous and binodal charge distributions, and the system will finally cross over to metallic behaviour. Although we use fractional charges in the Monte Carlo simulations, quantum effects are completely neglected in the approach presented here. Therefore, it is impossible to address the question of whether eigenstates of the electronic Hamiltonian are localized or extended. The calculations do, however, give an idea of the delocalization energy that has to be created by the formation of bands in order to overcome the splitting between a localized and a delocalized charge distribution. Whenever the M^0 bands are narrow or eigenstates below the Fermi level are highly localized, electron–electron interaction will play an additional rôle [15, 16]. The on-site electron–electron interaction, manifest in the Hubbard spin-pairing energy U, prevents the system studied here from further lowering its energy by means of the disproportionation $2M_0 \rightarrow M^+ + M^-$.

It is highly desirable to check the validity of the principle of maximum charge separation postulated in this work for systems that show a more refined parametrization scheme than the restricted primitive model used here. One of these schemes, the unrestricted primitive model of non-equi-sized charged hard spheres can be approached within the MSA, like its restricted counterpart [23], although it lacks the simple analytical tractability of the RPM. The MSA coupling constant, Γ, and the energies $\Delta U(\Gamma)$ and $\Delta F(\Gamma)$ would have to be evaluated numerically. Thus, the use of simple analytical arguments, as applied in the second section, becomes extraordinarily difficult.

As a large variety of systems that exhibit electronic degrees of freedom are dominated by Coulombic interactions, the *principle of maximum charge separation* will not be restricted to metal–molten-salt solutions. The intimately related liquid ionic alloys [32]—with Cs_yAu_{1-y} as the most prominent example—and compensated doped semiconductors like $Si{:}P_xB_y$ or metal oxides at high temperatures like $SrFe(III, IV)O_{3-\Delta}$ ($0 \leqslant \Delta \leqslant 1/2$ [33]) that cannot be described within the model of non-interacting small polarons are candidates worth inspecting from this point of view. Highly diluted systems, on the other hand, are characterized by a small MSA screening constant Γ and a small energy difference between homogeneous and heterogeneous charge distributions. Here, concentration-independent polarization terms of the type $V_{\mathrm{pol}} \propto z^2/\epsilon\sigma$ will dominate the energetics of the system, but will nevertheless lead to an identical charge distribution.

Acknowledgments

It is a pleasure to thank W Freyland and D Nattland for fruitful discussions and the Fonds der Chemischen Industrie for partial financial support.

References

[1] Freyland W 1990 *J. Non-Cryst. Solids* **117+118** 613
Freyland W 1994 *Z. Phys. Chem.* **184** 139
Freyland W 1995 *The Metal–Nonmetal Transition Revisited* ed P P Edwards and C N R Rao (London: Taylor and Francis)
[2] Jal J F, Mathieu C, Chieux P and Dupuy J 1990 *Phil. Mag.* B **62** 351
Hily L, Dupuy J, Jal J F and Chieux P 1994 *Rev. Int. Hautes Temp. Réfract. Fr.* **29** 1
[3] Warren W W, Sotier S and Brennert G F 1984 *Phys. Rev.* B **30** 65
[4] Bredig M A 1964 *Molten Salt Chemistry* ed M Blander (New York: Wiley-Interscience) and references therein

Nattland D, Heyer H and Freyland W 1986 *Z. Phys. Chem.* **149** 1
[5] Schindelbeck T and Freyland W 1995 *J. Phys.: Condens. Matter* **7** L469
Schindelbeck T and Freyland W 1996 *J. Chem. Phys.* **105** 4448
[6] Nattland D, Rauch Th and Freyland W 1993 *J. Chem. Phys.* **98** 4429
von Blanckenhagen B, Nattland D, Bala K and Freyland W 1999 *J. Chem. Phys.* at press
For Na–NaI, see von Blanckenhagen B, Nattland D and Freyland W 1994 *J. Phys.: Condens. Matter* **6** L179
[7] Juchem R, Nattland D and Freyland W 1993 *J. Non-Cryst. Solids* **156–158** 763
Nattland D, von Blanckenhagen B, Juchem R, Schellkes E and Freyland W 1996 *J. Phys.: Condens. Matter* **8** 9309
Juchem R 1995 Spektroellipsometrische Untersuchungen zum Metall-Nichtmetall-Übergang in K_xKCl_{1-x}-Schmelzen *PhD Thesis* Universität Karlsruhe
[8] Steininger R 1993 Untersuchungen zur mikroskopischen Struktur und Elektronenlokalisation in K_xKCl_{1-x}-Schmelzen mit Röntgenkleinwinkelstreuung *PhD Thesis* Universität Karlsruhe
Blessing J 1996 Röntgenkleinwinkelstreuung in $K_x(KCl)_{1-x}$-Schmelzen bei *in situ* coulometrischer Metalldotierung *PhD Thesis* Universität Karlsruhe
[9] Bernard J, Blessing J, Schummer J and Freyland W 1993 *Ber Bunsenges. Phys. Chem.* **97** 177
[10] Koslowski Th 1997 *J. Chem. Phys.* **106** 7241
[11] Parrinello M and Rahman A 1984 *J. Chem. Phys.* **80** 860
[12] Selloni A, Carnevali P, Car R and Parrinello M 1987 *Phys. Rev. Lett.* **59** 823
Selloni A, Carnevali P, Car R and Parrinello M 1987 *J. Phys. Chem.* **91** 4947
Fois E S, Selloni A, Parrinello M and Car R 1988 *J. Phys. Chem.* **92** 3268
Silvestrelli P L, Alavi A, Parrinello M and Frenkel D 1996 *Phys. Rev.* B **53** 12 750
[13] Anderson P W 1958 *Phys. Rev.* **109** 1492
[14] Logan D E and Siringo F 1992 *J. Phys.: Condens. Matter* **4** 3695
[15] Siringo F and Logan D E 1991 *J. Phys.: Condens. Matter* **3** 4747
[16] Koslowski Th and Logan D E 1994 *J. Phys. Chem.* **98** 9146
[17] Dijkstra M, Hansen J-P and Meroni A 1994 *J. Phys.: Condens. Matter* **6** 3695
[18] Holzhey C and Schirmacher W 1988 *Z. Phys. Chem.* **156** 163
[19] Beck U, Koslowski Th and Freyland W 1996 *J. Non-Cryst. Solids* **205–207** 52
[20] Ginoza M 1986 *J. Phys. Soc. Japan* **55** 95
Ginoza M 1986 *J. Phys. Soc. Japan* **55** 1782
Ginoza M 1990 *Mol. Phys.* **71** 145
[21] Yurdabak D, Akdeniz Z and Tosi M P 1994 *Nuovo Cimento* D **16** 307
[22] See e.g., Hansen J-P and MacDonald I R 1986 *Theory of Simple Liquids* 2nd edn (London: Academic) p 110
[23] Blum L and Høye J S 1977 *J. Phys. Chem.* **81** 1311
[24] Allen M P and Tildesley D J 1987 *Computer Simulations of Liquids* (Oxford: Clarendon)
[25] Adams D J 1979 *Chem. Phys. Lett.* **62** 329
Adams D J 1983 *J. Chem. Phys.* **78** 2585
Adams D J 1979 *Chem. Phys. Lett.* **62** 329
Adams D J 1983 *J. Chem. Phys.* **78** 2585
[26] Garbade K and Freyland W 1988 *Ber. Bunsenges. Phys. Chem.* **92** 1131
[27] Martin M, Marcus G, Chen Bin and Siepmann J I 1998 *J. Chem. Phys.* **108** 3383
[28] Koslowski Th 1996 *Ber. Bunsenges. Phys. Chem.* **100** 95
[29] Koslowski Th 1998 *Ber. Bunsenges. Phys. Chem.* **102** 1128
[30] We would like to note that an ideal mixture would be represented by $\Delta E(x) = \Delta E(x = 0)(1 - x)(2 - x)$ instead of the simple linear behaviour, as in the representation of the energy per formula unit as a function of x.
[31] See e.g., Cox P A 1987 *The Electronic Structure and Chemistry of Solids* (Oxford: Oxford University Press) p 45
[32] Warren W W 1985 *The Metal–Nonmetal Transition* ed P P Edwards and C N R Rao (London: Taylor and Francis)
[33] Hombo J, Matsumoto Y and Kawano T 1990 *J. Solid State Chem.* **84** 138
Mitsusaki J, Okayasu M, Yamauchi S and Fueki K 1992 *J. Solid State Chem.* **99** 166
Wimann S and Becker K D 1996 *Solid State Ion.* **89** 279